04

Investigation of gas temperature field in the pulsed electric discharge trace

© V.A. Lashkov,[1] Yu.V. Dobrov,[1] M.E. Renev,[1] I.Ch. Mashek,[1] N.Zh. Dzhaichibekov,[2] B.S. Shalabayeva[2]

[1] St. Petersburg State University,
St. Petersburg, Russia
[2] Gumilyov Eurasian National University,
010000 Nur-Sultan, Republic of Kazakhstan
e-mail: youdobrov@gmail.com

Received November 19, 2021
Revised December 14, 2021
Accepted December 24, 2021

This article devoted to the study of gas heating in the region of an electric interelectrode discharge. The dynamics of local heating is studied using numerical methods and experimentally using an interferometer. The research results make it possible to evaluate the change in the temperature distribution in the cross section of the discharge track, the dynamics of the maximum heating temperature and the size of the heated area.

Keywords: pulsed interelectrode discharge, low-temperature plasma, gas heating.

DOI: 10.21883/TP.2022.04.53601.294-21

Introduction

Active control over supersonic gas flows by local energy input is an important and long-range objective of current plasma aerodynamics. Local energy inputs into a supersonic gas flow allow one to alter the nature of flow around various bodies [1–6]: reduce the drag coefficient; increase the lift coefficient, thus increasing the lift-to-drag ratio; improve aircraft control; intensify mixing; and alter the boundary-layer flow regime. Energy may be introduced into an oncoming supersonic flow by various types of discharges [7–11]: laser spark, microwave discharge, electric interelectrode discharge, and dielectric barrier discharge.

The efficiency of conversion of the supplied electric energy into thermal gas energy is a crucial issue in the application of a heated channel in aerodynamics [6]. In addition to thermal influences, the structure of gas flow around an aerodynamic body may be affected by the non-equilibrium state of gas in a channel. This effect is especially pronounced at high Mach numbers of the oncoming flow [12].

The present study is focused on the determination of thermodynamic parameters of the trace of a channel heated by an electric interelectrode discharge and on the examination of temperature and geometry dynamics. Experiments were performed, and their results were compared with the numerical modeling data. Two primary phases may be distinguished in the discharge dynamics: the active phase, when a certain electric voltage is applied to electrodes and a plasma channel with gas in a non-equilibrium state forms, and the passive phase characterized by the transition of gas in the channel to an equilibrium state. The channel geometry and the distribution of power of plasma heating of the medium were determined in the section focused on the active discharge phase. These data were used to calculate the evolution of the channel trace in the passive phase. Particular attention was paid to the passive phase, since a channel trace heated after a discharge is often used in aerodynamic applications to modify the gas flow. The primary objective of the study is to establish the relation between electric parameters of an interelectrode discharge and the temperature of gas heating in the discharge trace.

1. Procedure of the experimental study of parameters of the channel trace

The discharge was produced in an experimental chamber by applying a voltage (20−25 kV) pulse with a duration of $3\,\mu$s via a ballast resistance of $800\,\Omega$ to electrodes. Experiments were conducted in air under atmospheric pressure. The distance between point–point electrodes was 6 mm. The maximum current of the active discharge phase was 25 A.

According to preliminary estimates, the thermal trace of the studied discharge introduces insignificant phase optical disturbances into the medium (the trace has a small linear size, and the magnitude of its heating is modest). Since double-beam interferometers are practically inapplicable in this case, a multibeam intrachamber Fabry–Pérot interferometer, which was characterized in [13], was used in the study.

The interferometer with a baseline of 0.2 m and an optical diameter of 0.09 m was illuminated via an IAB-450 instrument by a single-frequency helium–neon LGN-303 laser with an output power of 1 mV, a wavelength of 632.8 nm, and a relative frequency deviation below 10^{-10}. The interference pattern was recorded with a high-speed intensified PCO DiCAM-PRO GaAs P46 camera with a minimum

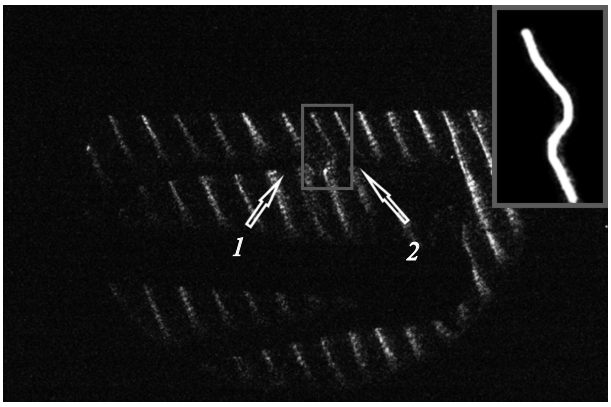

Figure 1. General interference pattern 140 μs after the discharge: *1* — cathode, *2* — anode.

exposure time of 5 ns. The typical exposure time in our experiments was on the order of 1 μs. The delay time between the exposure and the onset of discharge varied from 50 to 1000 μs.

2. Results of the experimental study of gas parameters in the discharge trace

A substantial concentration of electrons remaining in the channel after the active discharge phase may exert a significant influence on the results of interferometric measurements. However, since the characteristic relaxation time under atmospheric pressure is on the order of 1 μs [14], the influence of the electronic component was neglected in measurements of the channel temperature on large time scales. It was assumed that the shape of the region heated by the discharge is close to an axially symmetric one. The procedure detailed in [15] was applied to determine the temperature distribution in the cross section of the discharge trace.

Figure 1 presents an example interference pattern recorded with the interferometer 140 μs after the discharge.

The shaded regions in Fig. 1 correspond to the electric lead cable and the case to which electrodes are secured. The region of the interference pattern selected (using a graphics editor) for subsequent analysis is shown in the upper right corner.

The processing technique for interferometric lines, which was detailed in [15], was used to determine the variation of gas temperature T in the cross section of the discharge trace. The measurement results revealed that the maximum gas temperature on the discharge trace axis at 140 μs was $T_{\max} = 333$ K. The standard deviation of this estimate did not exceed 30 K. The characteristic size of the thermal trace estimated at half the maximum temperature was $S_5 = 2.2 \pm 0.3$ mm in this case.

The temporal variation of temperature on the axis of the discharge trace is presented in Fig. 2, *a*. Figure 2, *b* shows the temporal dependence of channel heating $\alpha = T_h/T_{\max}$, where T_h is the surrounding gas temperature. This parameter is often used in computer modeling of the interaction of a heated channel with a shock layer on a supersonic body [1,2]. The obtained results demonstrate that channel heating parameter α varied within the 0.8–0.95 range in the conditions of our experiments within the time interval of 50–1000 μs.

The temperature drops to 310 K by 1000 μs. Apparently, this occurs due to the dissipation of heat from the channel in the environment. This is also confirmed by the fact that parameter S_{50} increases with time elapsed from the onset of discharge (Fig. 3). The results of experiments revealed that parameter S_{50} increases almost linearly. At the time point located 1000 μs after the discharge, parameter S_{50} increases to approximately 14 mm.

3. Numerical modeling

3.1. Active discharge phase

Models of an interelectrode low-temperature plasma discharge in gas at rest have been proposed in a number of studies (see, e.g., [14,16–19]). They are used to solve various problems: examine the reasons behind streamer branching and calculate the parameters of the ionized region and the thermal, chemical, and force impact.

In the present study, self-consistent numerical calculations were performed in the 2*D* axially symmetric geometry for a pulsed interelectrode discharge in standard air at rest. The geometry of the computational domain is presented in Fig. 4. The electrode system consisted of two copper needle electrodes. A pulsed voltage $U_0(t)$ source (20 kV, the leading edge width was 200 ns) was connected to the system via resistance $R = 800\,\Omega$.

The following equations were used to calculate the discharge parameters.

The Poisson's equation:

$$-\varepsilon_0 \Delta\varphi = \rho_{ch},\ \rho_{ch} = |e|(n^+ - n_e - n^-),$$

where ε_0 is the electric constant; φ is the electric potential; ρ_{ch} is the electric charge density; $|e|$ is the elementary charge; n_+, n_-, n_e are the densities of all positive and negative ions and electrons; and $\mathbf{E}$ is the electric-field vector.

The continuity equation was used to calculate the density of electrons:

$$\frac{\partial n_e}{\partial t} + (\nabla, \mathbf{J}_e) + (\mathbf{V}_g, \nabla)n_e = S_e,\ \mathbf{J}_e = -b_e\mathbf{E}n_e - \nabla D_e n_e,$$

where $\mathbf{J}_e$ is the electron flux vector, $\mathbf{V}_g$ is the velocity of motion of the medium, S_e is the electron source, and b_e and D_e are the mobility and diffusion coefficients of electrons.

The equation of electron energy transfer:

$$\frac{\partial n_e\psi}{\partial t} + (\nabla, \mathbf{J}_\psi) + (\mathbf{E}, \mathbf{J}_e) + (\mathbf{V}_g, \nabla)n_e\psi = I^i_{pot}S^{in}_i - Q_e,$$

$$\mathbf{J}_\psi = -b_e\mathbf{E}n_e\psi - \nabla D_e n_e\psi,$$

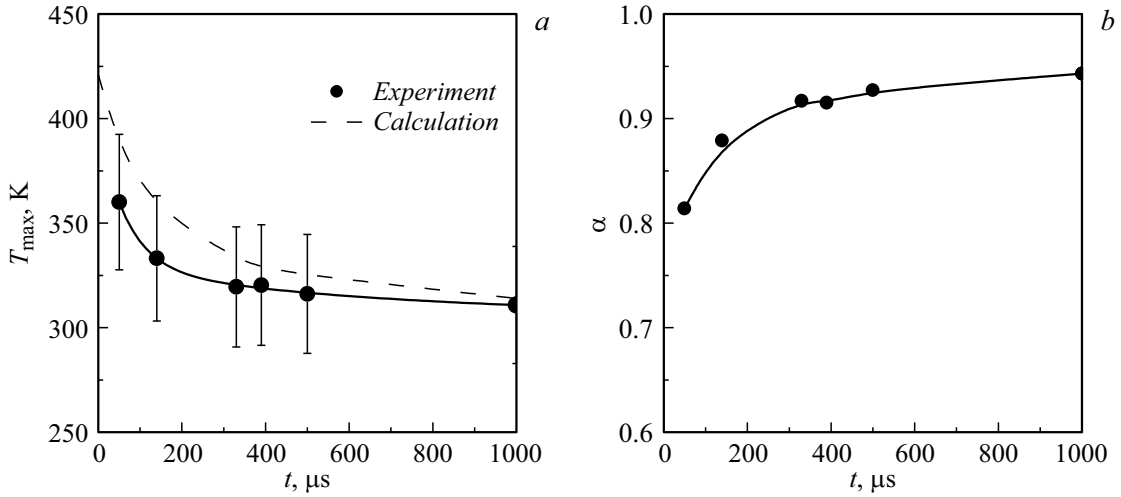

Figure 2. *a* — Variation of gas temperature T_{max} on the heated channel axis with time elapsed from the onset of discharge; *b* — temporal dependence of channel heating parameter α.

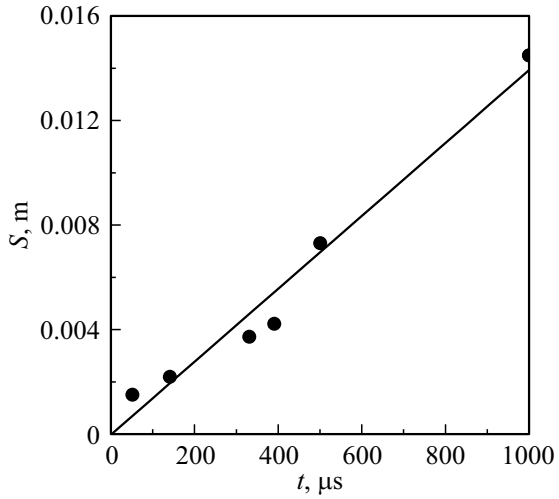

Figure 3. Distance from the discharge axis to the point where the gas temperature falls to 50% of the maximum temperature.

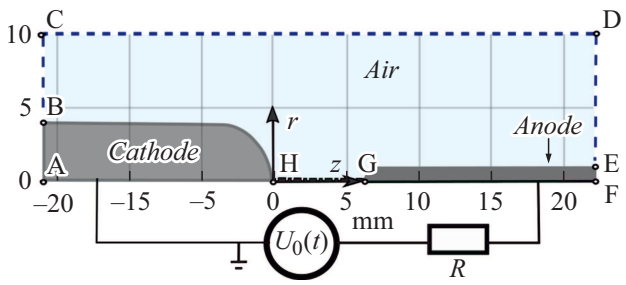

Figure 4. Geometry of the computational domain.

where $\mathbf{J}_\psi$ is the energy flux vector of the electron gas, ψ is the average energy of electrons, I^i_{pot} is the potential of reaction i, S^{in}_i is the rate of reactions in inelastic interactions, and Q_e is the power of medium heating due to elastic collisions with electrons.

Maxwell–Stefan equations:

$$\rho_g\left(\frac{\partial}{\partial t}+(\mathbf{V}_g,\nabla)\right)\omega_i=(\nabla,\rho\omega_i\mathbf{V}_i)+S_i,$$

$$\mathbf{V}_i=D_i\nabla(\ln\omega_i+\ln M_n)-z_i b_i\mathbf{E},$$

where ρ_g is the density of the medium; ω_i is the mass fraction of particles type i; $\mathbf{V}_i$ is the velocity of motion of particles type i; S_i is the source of particles type i; D_i, b_i, and z_i are the coefficients of diffusion and mobility in the electric field and the charge number of particles type i; and M_n is the average molar mass.

The photon transfer equation and the determination of the photoionization reaction rate [17]:

$$\frac{c}{-\lambda_{13.6}}\Delta n_{ph-13.6}+\lambda_{13.6}c=S_{N_2^{13.6}},$$

where c is the speed of light, $\lambda_{13.6}$ is the coefficient of absorption of photons by pure oxygen, $n_{ph-13.6}$ is the density of photons with an energy of 13.6 eV, $S_{N_2^{13.6}}$ is the source of excited (13.6 eV) nitrogen molecules, and $S_i^{ph-13.6}$ is photoionization.

The Navier–Stokes equation and the equation of thermal energy transfer:

$$\rho_g\left(\frac{\partial}{\partial t}+(\mathbf{V}_g,\nabla)\right)\mathbf{V}_g=$$

$$-\nabla p_g+\mu_g\left(\Delta\mathbf{V}_g+\frac{1}{3}\nabla(\nabla,\mathbf{V}_g)\right)+\rho_{ch}\mathbf{E},$$

$$\rho_g C_p\left(\frac{\partial}{\partial t}+(\mathbf{V}_g,\nabla)\right)T_g-\nabla(k_g\nabla T_g)=Q_+ + Q_{reac}+Q_e,$$

where p_g is the air pressure, μ_g is the gas viscosity, C_p is the specific thermal capacity of the medium under constant

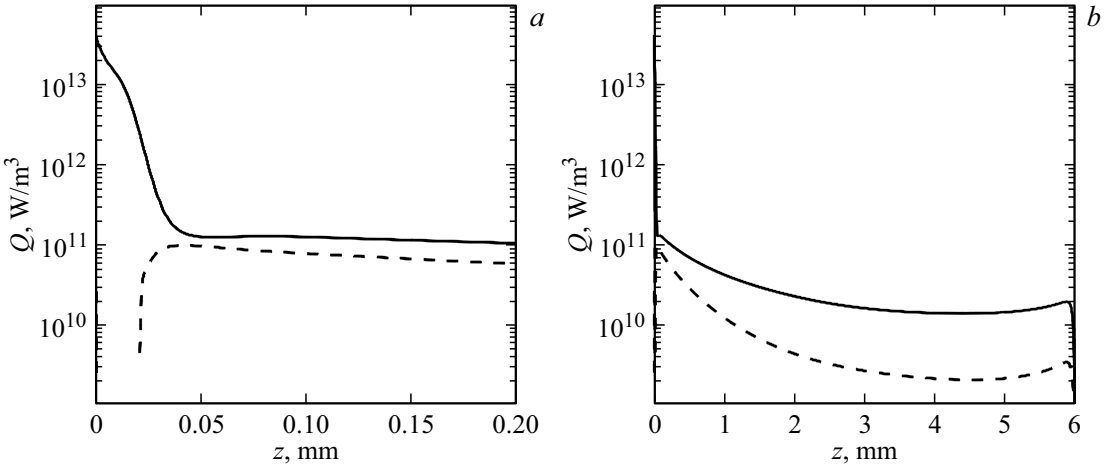

Figure 5. Distributions of power of heating at the time point of 260 ns by the ionic current (solid curve) and plasma reactions (dashed curve): *a* — near the cathode, *b* — entire gap.

pressure, T_g is the gas temperature, k_g is the thermal conductivity of the medium, and Q_+ and Q_{reac} are the powers of heating of the medium due to the drift motion of ions and reactions (recombination, relaxation, dissociation, etc.).

Approximations detailed in [20] were used in the presented model. The reactions of dissociation and associative ionization in air at high temperature were taken from [21]. The recombination and relaxation reactions were characterized in [16,22]. The heating powers were determined in accordance with [16]. The following types of particles were considered: e, O_2, O_2^+, O_2(a1d), O, O^+, O^-, N_2, N_2^+, N_2a, N_2A, N, N^+, NO, NO^+, and photons with an energy of 13.6 eV.

At the initial time, a uniform natural density of seed electrons and oxygen ions (10^{13} 1/m^3) is present between the electrodes.

The results of calculations demonstrated that a discharge in these conditions is initiated in 250 ns. Figure 5 shows the spatial distributions of volumetric powers of heating by the ionic current (solid curve) and plasma reactions (dashed curve) calculated at the time point of 260 ns. The calculated Joule heating of plasma by the ionic current is as high as $5 \cdot 10^{13}$ W/m^3 in the near-cathode layer (Fig. 5, *a*), which has a thickness below 0.05 mm, and three orders of magnitude lower outside of this layer (Fig. 5, *b*). The Joule heating outside of the near-cathode layer is 3–10 times more significant than the plasmachemical heating by reactions. The average overall heating power in a channel with a radius of 1 mm is approximately equal to $4.4 \cdot 10^{10}$ W/m^3. This value is established soon after the initiation of a discharge and closure of the interelectrode gap. The power of heating by elastic electron collisions is negligible and is not presented in the figures.

Thus, the results of calculations for the initial stage of a high-voltage interelectrode discharge in a medium at rest revealed that the average volumetric power of Joule heating in a cylindrical channel 2 mm in diameter is $4.4 \cdot 10^{10}$ W/m^3. This value was used to model the gas dynamics of the passive discharge phase.

3.2. Passive discharge phase

The calculated data for the active discharge phase were used to model the gas dynamics. Numerical modeling was performed in the ANSYS FLUENT package. An axially symmetric problem was considered within the model of an ideal viscous gas; the system of Navier–Stokes equations was solved to characterize the gas dynamics:

$$\frac{\partial \rho}{\partial t} + \nabla(\rho \mathbf{V}) = 0,$$

$$\frac{\partial}{\partial t}(\rho \mathbf{V}) + \nabla(\rho \mathbf{V}\mathbf{V}) = -\nabla p + \nabla(\bar{\bar{\boldsymbol{\tau}}}),$$

$$\frac{\partial}{\partial t}(\rho E) + \nabla\big(\mathbf{V}(\rho E + p)\big) = \rho q + \nabla(\lambda \nabla T),$$

where ρ is density, $\mathbf{V}$ is the velocity vector, p is pressure, τ is the stress tensor, E is the total energy, q is the source energy term, λ is the thermal conductivity coefficient, and T is temperature. The ideal gas law and the k-epsilon turbulence model were used to close the system of equations.

The problem was solved with the following initial conditions: a standard medium pressure and a temperature of 293 K. The region of energy input was a cylinder 6 mm in length and 2 mm in diameter. This region was heated with a power of $4.4 \cdot 10^{10}$ W/m^3 for 2.7 μs. The energy input was on the order of 2.5 mJ. The supplied electric energy measured experimentally was 22 mJ. Thus, the efficiency of heating of the gas channel with an electric discharge was 11%. Figure 6, *a* shows the distribution of temperature along radius R in the central section of the heated channel at different time points. Figure 6, *b* presents the comparison

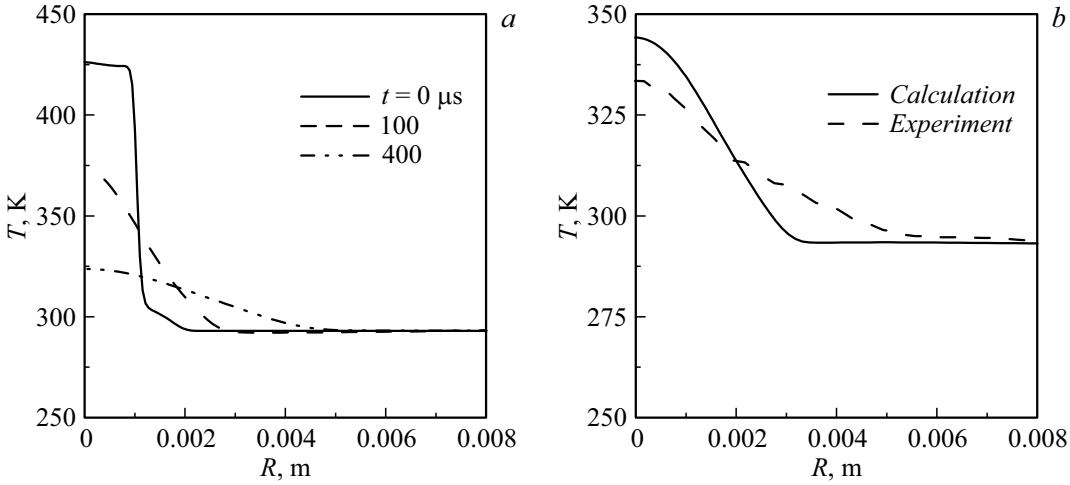

Figure 6. *a* — Temperature distribution in the cross section at different time points after the discharge; *b* — temperature distribution in the cross section 140 μs after the discharge.

of calculated and experimental data obtained 140 μs after the discharge.

The gas temperature on the channel axis decreases with time from 427 K after the active discharge phase to 373 K within 100 μs (see the dashed curve in Fig 6, *a*). It may be noted that the results of calculations agree fairly well with the experimental data within the accuracy of determination of the examined parameters.

Conclusion

The evolution of gas temperature in the trace of a pulsed electric interelectrode discharge was studied experimentally. New data on the dynamics of gas temperature were obtained using the interferometric method. Numerical modeling of the active discharge phase was performed. The gas temperature in the passive discharge phase was calculated based on the data obtained in modeling of the active phase. The experimental data are in a satisfactory agreement with the calculated ones.

The calculated gas temperature on the axis channel after the active phase in the discharge trace was 427 K in the studied conditions. This corresponds to parameter $\alpha = 0.68$. The temperature of gas in the channel decreases fairly rapidly with time elapsed from the moment of discharge: it drops approximately by 100 K within 140 μs. The characteristic size of the heated region increases linearly with time. In the studied range of parameters, this region grew to 14 mm within 1 ms after the discharge. The efficiency of utilization of the energy of a pulsed electric discharge for gas heating in the channel trace was on the order of 10%.

Acknowledgments

Equipment of the Computing Center at the St. Petersburg University Research Park was used in the studies.

Funding

The study was supported financially by the Committee of Science of the Ministry of Education and Science of the Republic of Kazakhstan. Project: AP09562291.

We acknowledge financial support from the St. Petersburg University received as a part of project Event 1 (id 84912260).

Conflict of interest

The authors declare that they have no conflict of interest.

References

[1] P.Yu. Georgievskii, V.A. Levin. Tr. MIAN SSSR, **186**, 197 (1989).

[2] O.A. Azarova, V.G. Grudnitsky, Yu.F. Kolesnichenko. Mat. Model., **18** (1), 79 (2006).

[3] S.M. Aulchenko, V.P. Zamuraev, A.P. Kalinina. J. Appl. Mech. Tech. Phys., **50** (5), 760 (2009).

[4] O.A. Azarova, D. Knight, Yu.F. Kolesnichenko. Prog. Flight Phys., **5**, 139 (2013). DOI: 10.1051/eucass/201305139

[5] N. Kianvashrad, D. Knight, S.P. Wilkinson, A. Chou, G.B. Beeler, M. Jangda. *Effect of Of-Body Laser Discharge on Drag Reduction of Hemisphere Cylinder in Supersonic Flow-Part II.* AIAA 2018-1433. AIAA Aerospace Sciences Meeting, Kissimmee, Florida, 8–12 January (2018). DOI: 10.2514/6.2018-1433

[6] V.A. Lashkov, A.G. Karpenko, R.S. Khoronzhuk, I.Ch. Mashek. Phys. Plasmas, **23**, 052305 (2016). DOI: 10.1063/1.4949524.

[7] V.A. Lashkov, I.Ch. Mashek, Yu.I. Anisimov, V.I. Ivanov, Yu.F. Kolesnichenko, M.I. Ryvkin, A.A. Gorynya. *Gas Dynamic Effect of Microwave Discharge on Supersonic Cone Shaped Bodies.* AIAA-2004-671. 42nd AIAA Aerospace Sciences Meeting and Exhibit, Reno, Nevada, 5–8 January (2004). DOI: 10.2514/6.2004-671

[8] P.-Q. Elias, N. Severac, J.-M. Luyssen, J.-P. Tobeli, F. Lambert, et al. *Experimental Investigation of Linear Energy Deposition Using Femtosecond Laser Filamentation in a $M = 3$ Supersonic Flow*. AIAA 2018-4896, Joint Propulsion Conference, Cincinnati, Ohio, 9–11 July (2018). DOI: 10.2514/6.2018-48962018
[9] Yu.V. Dobrov, V.A. Lashkov, I.Ch. Mashek, A.V. Mityakov, V.Yu. Mityakov, S.Z. Sapozhnikov, R.S. Khoronzhuk. Tech. Phys., **66** (2), 229 (2021). DOI: 10.1134/S1063784221020109
[10] Y.V. Dobrov, V.A. Lashkov, I.Ch. Mashek, R.S. Khoronzhuk. AIP Conf. Proceedings, **1959**, 050009 (2018). DOI: 10.1063/1.5034637
[11] P. Bletzinger, B.N. Ganguly, D. VanWie, A. Garscadden. J. Phys. D: Appl. Phys., **38**, R33 (2005). DOI: 10.1088/0022-3727/38/4/R01
[12] O.A. Azarova, A.V. Erofeev, T.A. Lapushkina. Tech. Phys. Lett., **43** (4), 405 (2017). DOI: 10.21883/PJTF.2017.08.44540.16598
[13] I.Ch. Mashek, Yu.I. Anisimov, V.A. Lashkov, Yu.F. Kolesnichenko. *Multibeam Interferometry of Self-Sustaining and Laser Induced MW Discharge in air*. AIAA 2005-790. 43rd AIAA Aerospace Sciences Meeting and Exhibit, Reno, Nevada, 10–13 January (2005). DOI: 10.2514/6.2005-790
[14] A.V. Samusenko, Yu.K. Stishkov. *Elektrofizicheskie protsessy v gazakh pri vozdeistvii sil'nykh elektricheskikh polei* (VVM, St. Petersburg, 2012), 649 pp (in Russian).
[15] G.I. Aseev. *Ispol'zovanie interferometra Makha-Tsendera dlya opredeleniya prostranstvennogo raspredeleniya pokazatelya prelomleniya i temperatury v plameni* (SarGU, Saratov, 2005) (in Russian).
[16] Yu.P. Raizer. *Fizika gazovogo razryada* (Intellekt, 2009), 691 pp (in Russian).
[17] U. Ebert, F. Brau, G. Derks, W. Hundsdorfer, C.-Y. Kao, C. Li, A. Luque, B. Meulenbroek, S. Nijdam, V. Ratushnaya, L. Schäfer, S. Tanveer. Nonlinearity, **24** (1), C1 (2011). DOI: 10.1088/0951-7715/24/1/C01
[18] N.St.J. Braithwaite. Plasma Sources Sci. Technol., **9** (4), 517 (2000). DOI: 10.1088/0963-0252/9/4/307/meta
[19] K. Kourtzanidis, L.L. Raja, S. Coumar, V. Lago. *Numerical Simulation of DC Glow Discharges for Shock Wave Modification*. AIAA 2016-2157. 54th AIAA Aerospace Sciences Meeting, San Diego, California, 4-8 January (2016). DOI: 10.2514/6.2016-2157
[20] M.E. Renev, Yu.V. Dobrov, V.A. Lashkov, I.Ch. Mashek. Vestnik St.Petersburg University. Mathematics. Mechanics. Astronomy, **54** (4), 428 (2021). https://doi.org/10.1134/S1063454121040154
[21] C. Park, J.T. Howe, R.L. Jaffe, G.V. Candler. J. Thermophys. Heat Transfer, **8** (1), 9 (1994). DOI: 10.2514/3.496
[22] A.I. Saifutdinov, E.V. Kustova, A.G. Karpenko, V.A. Lashkov. Plasma Phys. Rep., **45** (6), 602 (2019). DOI: 10.1134/S1063780X19050106